The pyramid wavefront sensor for the High Order Testbench (HOT)

E. Pinna[a], A. T. Puglisi[a], F. Quirós-Pacheco[a], L. Busoni[a], A. Tozzi[a], S. Esposito[a], E. Aller-Carpentier[b] and M. Kasper[b]

[a]Osservatorio Astrofisico di Arcetri, L.go E. Fermi n.5 - 50125 Firenze, Italy,
[b] European Southern Observatory, Karl-Schwarzschild-str. 2, 85748 Garching, Germany

ABSTRACT

The High Order Testbench (HOT) is a joint experiment of ESO, Durham University and Arcetri Observatory to built and test in laboratory the performance of Shack-Hartmann and pyramid sensor in a high-order correction loop using a 32x32 actuators MEMS DM. This paper will describe the pyramid wavefront sensor unit developed in Arcetri and now installed in the HOT bench at ESO premises. In the first part of this paper we will describe the pyramid wavefront sensor opto-mechanics and its real-time computer realized with a commercial Linux-PC. In the second part we will show the sensor integration and alignment in the HOT bench and the experimental results obtained at ESO labs. Particular attention will be paid to the implementation of the modal control strategy, like modal basis definition, orthogonalization on the real pupil, and control of edge actuators. A stable closed loop controlling up to 667 modes has been achieved obtaining a Strehl ratio of $90-93\%$ in H band.

Keywords: high-order adaptive optics, pyramid wavefront sensor, modal control.

1. INTRODUCTION

This paper describes a high-order Pyramid Wavefront Sensor (PS)[1] development in the framework of the JRA1 research program work package 3.8 named High Order Testbench (HOT)[2] . Briefly, this experiment is aimed at comparing the performance of a Pyramid sensor and a Shack-Hartmann[3] sensor in a high-order correction AO system using a 1000-actuators MEMS deformable mirror. Because of the limited stroke of the MEMS, the experiment uses phase screens whose low order aberrations have been reduced. Static low order aberrations are corrected using a bimorph mirror, namely a lab unit of the ESO MACAO curvature system.[4] This mirror provides real-time correction for tip and tilt that otherwise could saturate the MEMS. An opto-mechanical drawing of the HOT bench as developed at ESO is reported in Figure 1. The PS design is based on the PS developed for the LBT AO system.[5] The Arcetri Observatory AO group is responsible for the design, integration and laboratory test of the PS at ESO premises. The laboratory tests at ESO have been carried out in collaboration with the ESO AO group. The paper describes the opto-mechanical set-up of the PS, then the modal basis used to control the high order AO system, and finally it reports the laboratory results obtained in the last run at ESO.

2. PYRAMID WFS OPTO-MECHANICS

The PS optical design reported in fig. 2 was directly obtained from the LBT WFS optical design.[5] The input beam of the PS has to be a telecentric with an f/16.7 aperture. This input beam enables to have the correct pupils position and shape on the final WFS CCD camera. In order to pass from the delivered f/50 beam to the f/16.7 beam the WFS has an auxiliary refocusing system made up of two achromatic lenses that refocus the f/50 in an f/16.7 telecentric beam. These auxiliary lenses are labelled L1 and L2 in fig. 2. The input beam at F/50 is provided by the HOT bench foreoptics.

The HOT system pupil has a diameter equal to 31 MEMS actuator pitches. The actuator pitch of the MEMS is 0.34 mm. The PS optical configuration uses a 36mm focal-length camera lens to create pupil images having a nominal diameter of $744\,\mu m$ (31 pixels of the PS CCD having a pixel size of $24\,\mu m$). The pupil arrangement with respect to the actuator grid and subaperture grid is shown in fig. 3. The set of four pupil images created after the

Send correspondence to Enrico Pinna
E-mail: pinna@arcetri.astro.it, Telephone: +39 055 2752 207

Adaptive Optics Systems, edited by Norbert Hubin, Claire E. Max, Peter L. Wizinowich,
Proc. of SPIE Vol. 7015, 701559, (2008)
0277-786X/08/$18 · doi: 10.1117/12.789483

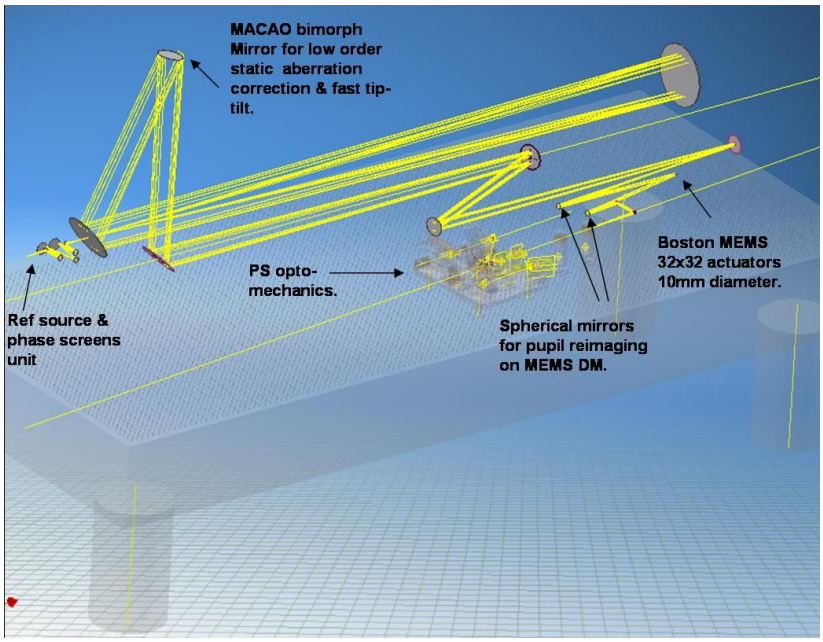

Figure 1. The figure shows the full optical set-up of the HOT bench realized at ESO. The main components of the system highlighted in the picture are: the MACAO mirror used for fast tip-tilt correction; the Boston MEMS with 1000 actuators used for the main AO loop and the PS board receiving a telecentric F/50 input beam from the bench foreoptics.

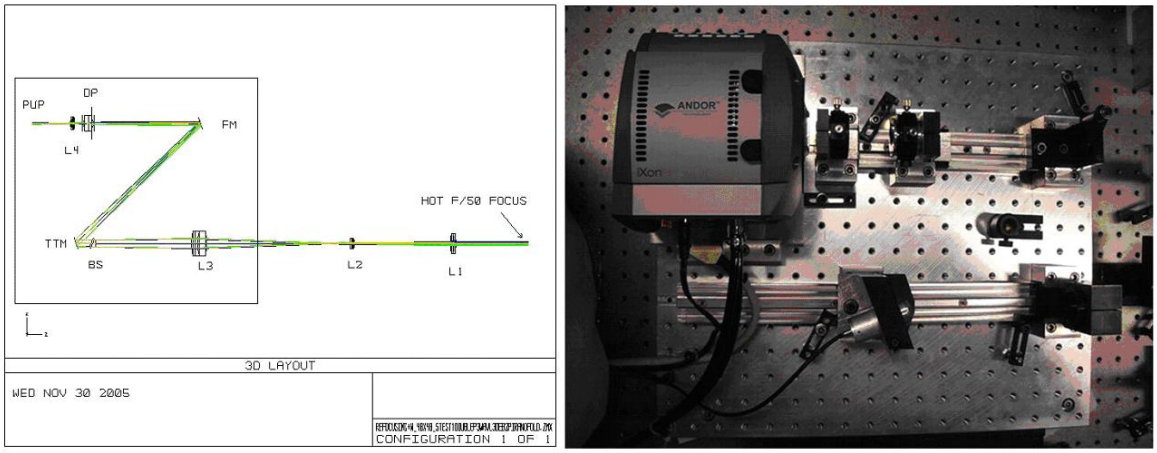

Figure 2. **Left:** The PS optical design of the HOT unit. The arrow before L1 shows approximately the f/50 beam focus position. L1 and L2 are the refocusing unit. The optics of the PWFS starts from L3. The box dimensions are 325x300mm. **Right:** The PS unit realized in Arcetri for the HOT experiment.

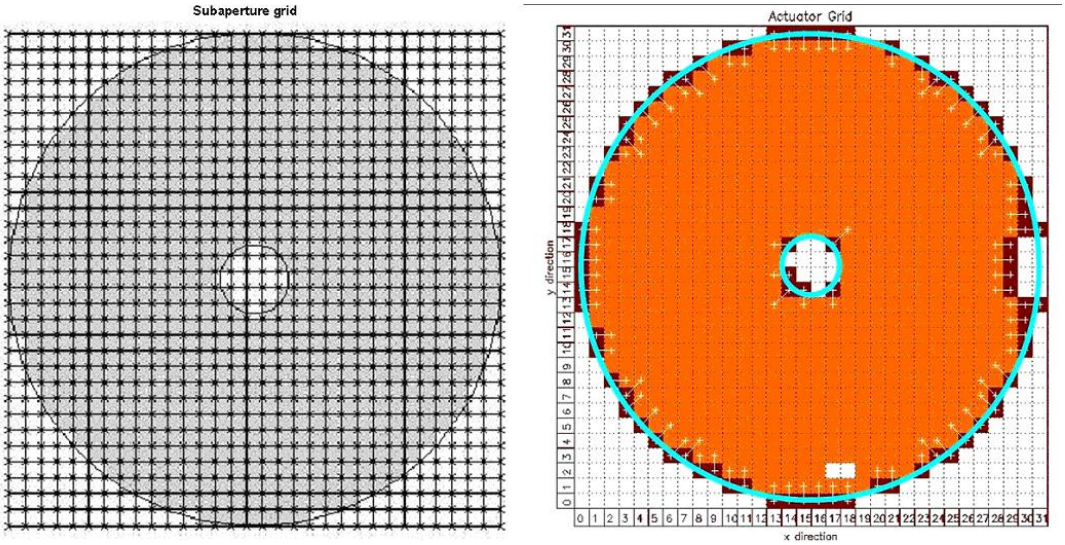

Figure 3. **Left:** the nominal registration of the PS subaperture grid is showed together with the HOT system pupil. Fried geometry is used in this case. **Right:** the actuator grid is shown together with the HOT pupil. The dark squares represent actuators driven as slaves during the closed loop operation. Defective actuators are shown in white.

pyramid by the camera lens are nominally placed on a square having a side of $985\,\mu m$. This corresponds to 41.0 pixels of the PS detector. To compensate for small errors in pupil magnification and rotation some laboratory procedures were developed. These procedures enable to estimate (a) the ratio between the pixel size and the actuator pitch, (b) the relative rotation between actuator grid and CCD pixel grid (c) the overall rotation of the four pupils set relative to the CCD pixel grid. In our last run, quantity (a) was adjusted to be 1 ± 0.03 slightly refocusing the camera lens; quantity (b) was found to be correctly aligned in the HOT bench set-up being less than 3.7^o, and quantity (c) was adjusted by rotating the pyramid reaching a value less than 1.4^o. A CCD averaged frame showing the four pupils arrangement together with the nominal arrangement is reported in fig. 4. Measured pupils are arranged in a square having a side of 42.0 ± 0.2 pixels. This number is not the design value of 41.0, but any separation with an integer number of pixels, that avoids pupil overlapping, will not affect the PS performances.

3. SYSTEM MODAL CONTROL

3.1 System modal basis

The modal basis created to control the system is based on KL modes projected onto the MEMS influence functions. The MEMS influence functions measured by ESO with an interferometer were actually used in this procedure. The modes were also orthonormalized in the HOT mask, taking into account the central obscuration and an additional masked area covering the defective actuators. Also, the tip-tilt components were projected out from all modes in order to control them separately with the TT mount of the MACAO mirror. The controlled actuators selected from the 32x32 actuators grid are showed in fig. 3. A total of 768 actuators were controlled, from which a set of 82 actuators (shown in dark gray in fig. 3) were controlled as slaves. Slave actuators were selected as the ones for which the 50% of their influence function FHWM lie outside the HOT mask. Hence, we controlled a total of 686 effective free actuators. It is important to mention that the slave-master information was also taken into account when creating the modal basis (i.e. when projecting the KL modes onto the MEMS influence functions). We verified that this approach effectively prevents the saturation of border actuators, as it happened with no-slaving control. Using this procedure to create a modal basis, we managed to compute a maximum of 667 orthonormal modes (665 HOT-KL modes + Tip and Tilt).

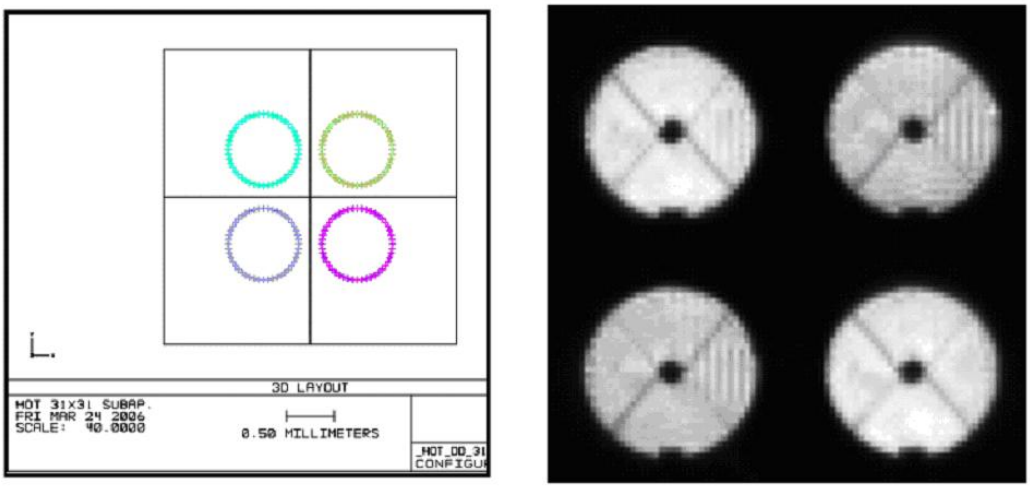

Figure 4. **Left:** The nominal arrangement of the four pupils on the PS CCD. **Right:** the four pupils image obtained averaging several CCD frames in closed loop.

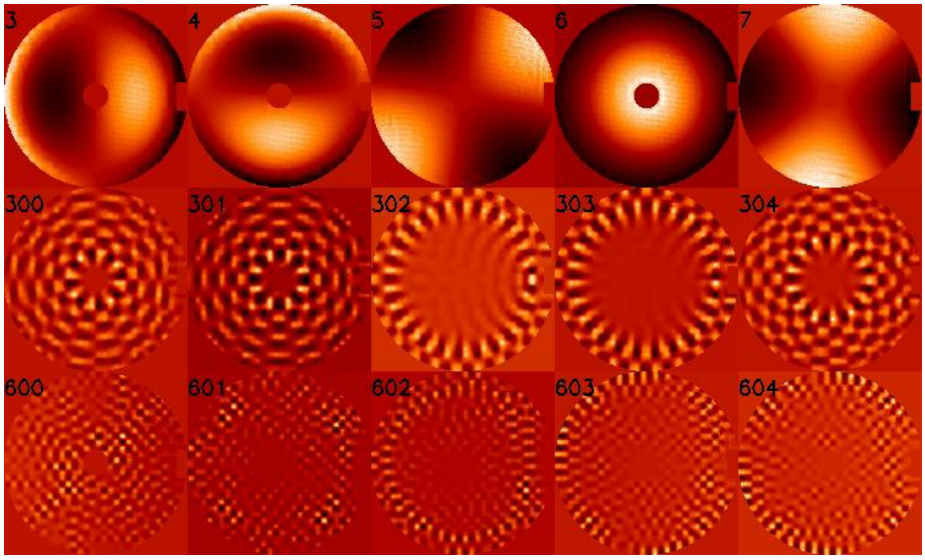

Figure 5. A sample of 15 modes that compose the modal basis used for the system control. The number on the top-left corner is the mode index. Notice the small rectangular region associated with the defective-actuator's mask.

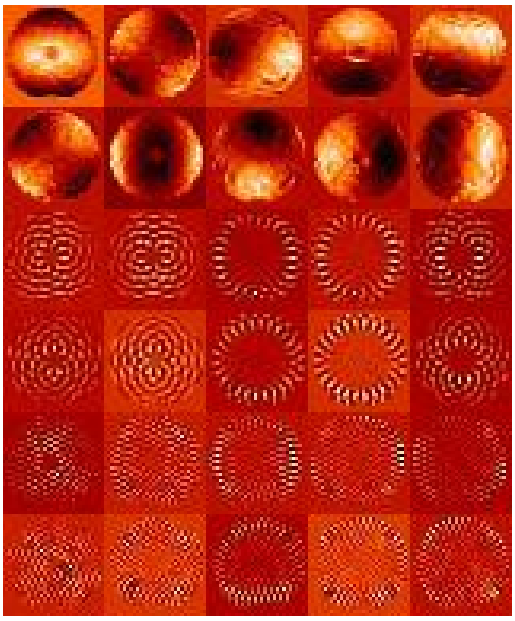

Figure 6. The PS signals obtained applying the 15 modes shown in fig. 5. Each mode is associated with a pupil map of the x-signals (top) and a second one for the y-signals (bottom). These are examples of the signals recorded in the interaction matrix of the system.

3.2 Interaction matrix measurements

After identifying the required modal basis for the considered pupil, we measured the system modal interaction matrix. The sensor signal for a given mode was measured taking the difference between the two signal frames acquired with the MEMS in +mode*amp and -mode*amp position where amp is an amplitude factor that was scaled as the square root of the mode number. This was done to prevent sensor's saturation due to the high signal amplitudes obtained from the higher spatial frequencies that characterize higher-number modes. However, this scaling was done up to mode 200. After this mode a constant amplitude was applied. To avoid lab optical disturbance due to local convection, slow drifts of the set-up, and all other possible slow system perturbations, we took the two exposures as short exposures one right after the other. Then, several couples were taken and averaged to provide a better estimate of the measured signal vector. In our case, the short-exposure time was set to $10\,ms$ and the time delay between short exposures was approximately $30\,ms$.

4. CLOSED-LOOP TESTS

Some closed-loop tests were done to measure the system performance in terms of PSF correction. The corrected PSF has been acquired using an IR camera in H band. The results we present here were obtained with the following configuration of the system: two phase screen counter-rotating at an equivalent speed of $3\,m/s$ while the CCD frame rate was $80\,Hz$. The gain of L3CCD was set to about 0.6 of the maximum gain allowed. In this situation, the L3CCD equivalent RON was measured to be about $3e^-$ against the nominal $0.5e^-$. The performance achieved in closed loop has been analyzed in terms of the modal residuals and the corrected PSF.

4.1 Modal residuals

We investigated the closed-loop performance for different flux levels. The open-loop and closed-loop modal standard deviation is reported in fig. 7 for the four considered levels of subaperture flux; namely 770, 153, 77, and 23 photoelectrons per subaperture and integration time. We estimated the modal rms values from a time sequence of open and closed-loop sensor signals retrieved from the real-time computer, and projected onto the

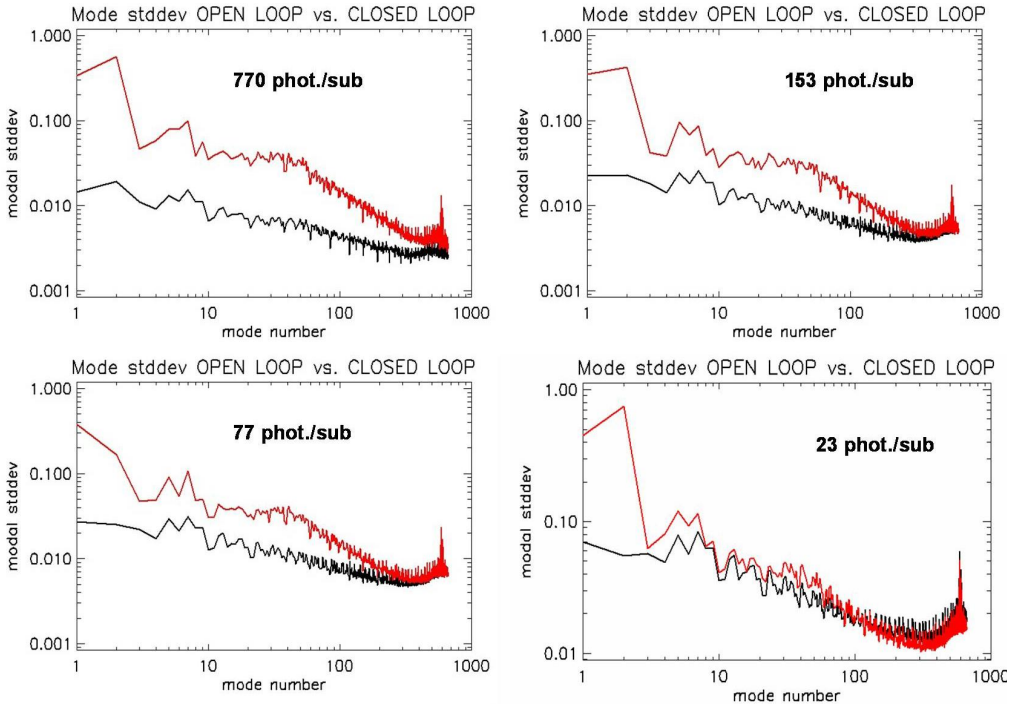

Figure 7. Plot of the modal standard deviation in open loop (gray line) and closed loop (black line) for four different flux levels.

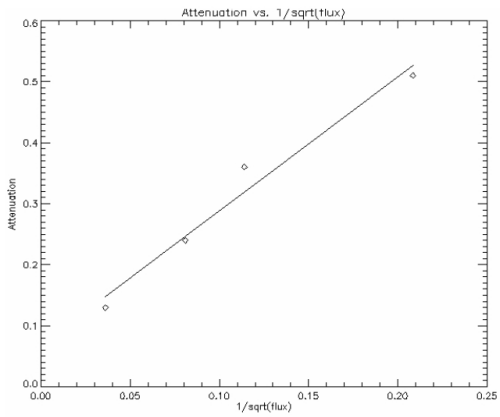

Figure 8. . Plot of wavefront rms attenuation as a function of 1/sqrt(flux).

modes using the reconstruction matrix. Note that the number of effectively corrected modes varies accordingly from a maximum of 667 at the highest flux level to a minimum of 200 at the fainter end. In order to improve the modal correction at lower flux levels, we will implement as a next step a modal gain optimization approach.[6]

The overall attenuation of the incoming wavefront, defined as the ratio of the closed loop wavefront rms divided by the open loop wavefront rms, has been evaluated for the four considered flux levels. Figure 8 summarizes the results. As expected, the overall attenuation scales with the square root of the total flux. The plot clearly show a linear relationship. Performing a fit on the data, a coefficient of wavefront rms attenuation versus square root of photons is found to be 2.19.

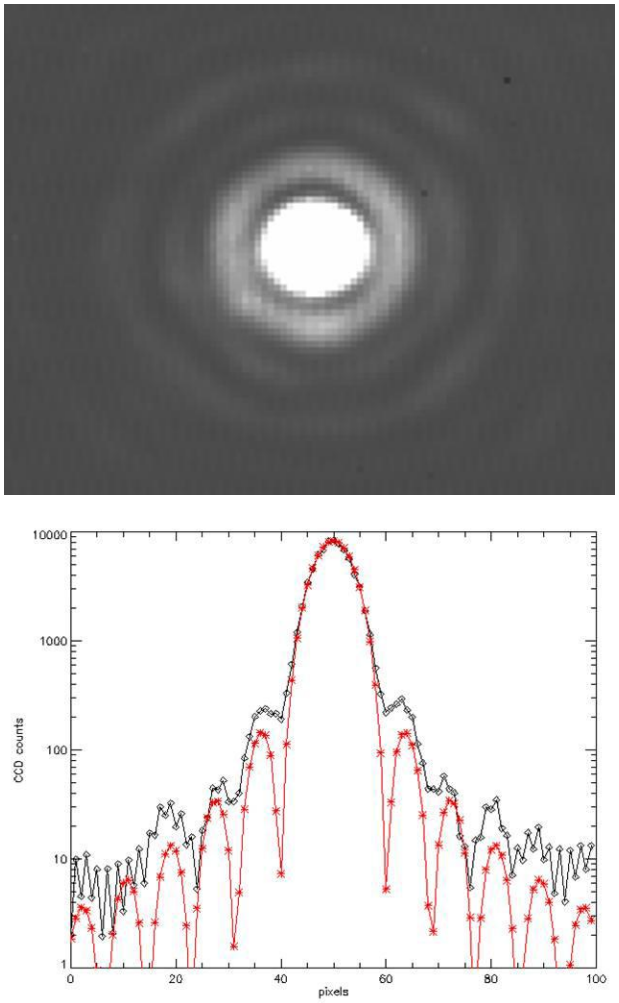

Figure 9. **Top:** PSF on the infrared camera (H band) obtained in closed loop with the high flux regime. **Bottom:** horizontal cut along the PSF peak, together with a theoretical Airy distribution (monochromatic) with the same geometry.

4.2 Corrected PSF

Let us present in this section an example of a corrected system PSF measured with the NIR camera in H band (pixel scale $\approx$ 5.2mas/pixel). The best PSF achieved was obtained for the highest flux level, and when correcting 667 modes. The measured PSF is shown in fig. 9. We determined that the contrast at a distance of 75mas is on the order of 1e3. The measured Strehl ratio is in between 90 and 93%.

5. CONCLUSIONS

A pyramid wavefront sensor with 30 sub-apertures in the pupil diameter has been designed, assembled and integrated in the High Order Testbench. The AO corrector, composed by a MEMS with 32X32 actuators plus a TT corrector, has been controlled with a basis of 667 modes. Closed loop tests have been performed in presence of atmospheric disturbances emulated by phase screens generating an equivalent seeing of 0.5″. The corrected PSF has been acquired with an infrared camera in the H band, reaching a Strehl ratio between 90 and 93%. The comparison between the modal standard deviation in open and closed loop shows that the system, when working in high flux regime, is able to correct all the 667 controlled modes.

The work at the HOT bench is still going on for a direct comparison between pyramid and Shack-Hartmann wavefront sensors. Soon a coronograph will be installed on the bench in order to study the performances when working with an extreme AO system. The present and further results will be relevant for the development of the future extreme AO instruments like SPHERE[7] and EPICS.[8]

REFERENCES

[1] Ragazzoni, R., "Pupil plane wavefront sensing with an oscillating prism," *Journal of Modern Optics* **43**, 289–293 (Feb. 1996).

[2] Vernet, E., Kasper, M., Vérinaud, C., Fedrigo, E., Tordo, S., Hubin, N., Esposito, S., Pinna, E., Puglisi, A., Tozzi, A., Basden, A. G., Goodsell, S. J., Love, G. D., and Myers, R. M., "Extreme adaptive optics system optimization with the high order test bench," in [*Advances in Adaptive Optics II*], Ellerbroek, B. L. and Bonaccini, D., eds., *Proceedings of the SPIE* **6272**, 62722K (2006).

[3] Aller-Carpentier, E., Kasper, M., Esposito, S., and Myers, R., "High order test bench for extreme adaptive optics system optimization," in [*Adaptive Optics Systems*], *Proc. of the SPIE* **7015** (2008).

[4] Arsenault, R., Alonso, J., Bonnet, H., Brynnel, J., Delabre, B., Donaldson, R., Dupuy, C., Fedrigo, E., Farinato, J., Hubin, N. N., Ivanescu, L., Kasper, M. E., Paufique, J., Rossi, S., Tordo, S., Stroebele, S., Lizon, J.-L., Gigan, P., Delplancke, F., Silber, A., Quattri, M., and Reiss, R., "MACAO-VLTI: An Adaptive Optics system for the ESO VLT interferometer," in [*Adaptive Optical System Technologies II. Proceedings of the SPIE*], Wizinowich, P. L. and Bonaccini, D., eds., *Presented at the Society of Photo-Optical Instrumentation Engineers (SPIE) Conference* **4839**, 174–185 (Feb. 2003).

[5] Esposito, S., Tozzi, A., Puglisi, A., Fini, L., Stefanini, P., Salinari, P., Gallieni, D., and Storm, J., "Development of the first-light AO system for the large binocular telescope," in [*Astronomical Adaptive Optics Systems and Applications*], Tyson, R. K. and Lloyd-Hart, M., eds., *Proceedings of the SPIE* **5169**, 149–158 (Dec. 2003).

[6] Gendron, E. and Lena, P., "Astronomical adaptive optics. 1: Modal control optimization," *Astronomy and Astrophysics* **291**, 337–347 (Nov. 1994).

[7] Fusco, T., Petit, C., Rousset, G., Sauvage, J.-F., Dohlen, K., Mouillet, D., Charton, J., Baudoz, P., Kasper, M., Fedrigo, E., Rabou, P., Feautrier, P., Downing, M., Gigan, P., Conan, J.-M., Beuzit, J.-L., Hubin, N., Wildi, F., and Puget, P., "Design of the extreme AO system for SPHERE, the planet finder instrument of the VLT," in [*Advances in Adaptive Optics II. Proceedings of the SPIE.*], **6272** (July 2006).

[8] Kasper, M., Verinaud, C., Beuzit, J.-L., Yaitskova, N., Hubin, N., Boccaletti, A., Dohlen, K., Fusco, T., Glindemann, A., Gratton, R., and Thatte, N., "EPICS: A Planet Hunter for the European ELT," in [*In the Spirit of Bernard Lyot: The Direct Detection of Planets and Circumstellar Disks in the 21st Century*], Kalas, P., ed. (June 2007).